Inorganic Chemistry

Article

The Electronic Structure of Inorganic Benzenes: Valence Bond and Ring-Current Descriptions

**Jeroen J. Engelberts,[†] Remco W. A. Havenith,[†] Joop H. van Lenthe,[†]
Leonardus W. Jenneskens,*,[‡] and Patrick W. Fowler[§,||]**

*Debye Institute, Theoretical Chemistry Group, Utrecht University, Paifualaan 8, 3584 CH Utrecht,
The Netherlands, Debye Institute, Organic Chemistry and Catalysis, Utrecht University,
Paifualaan 8, 3584 CH Utrecht, The Netherlands, and Department of Chemistry, University of
Exeter, Stocker Road, Exeter EX4 4QD, U.K.*

Valence bond (VB) theory and ring-current maps have been used to study the electronic structure of inorganic benzene analogues X_6H_6 (X = C (**1**), Si (**2**)), X_6 (X = N (**3**), P (**4**)), $X_3Y_3H_6$ (X,Y = B,N (**5**), B,P (**6**), Al,N (**7**), Al,P (**8**)), and $B_3Y_3H_3$ (Y = O (**9**), S (**10**)). It is shown that the homonuclear compounds possess benzene-like character, with resonance between two Kekulé-like structures and induced diatropic ring currents. Heteronuclear compounds typically show localization of the lone pairs on the electronegative atoms; Kekulé-like structures do not contribute. Of the heteronuclear compounds, only $B_3P_3H_6$ (**6**) has some benzene-like features with a significant contribution of two Kekulé-like structures to its VB wave function, an appreciable resonance energy, and a discernible diatropic ring current in planar geometry. However, relaxation of **6** to the optimal nonplanar chair conformation is accompanied by the onset of localization of the ring current.

1. Introduction

Benzene is the archetypal example of a molecule that possesses remarkable physical properties arising from its delocalized π-electrons. Historically, chemists have searched for other molecules that resemble benzene. Borazine ($B_3N_3H_6$ (**5**)) and boroxine ($B_3O_3H_3$ (**9**)) are examples that have been proposed: both are similar to benzene in geometry and in formal topology of the π-molecular orbitals. However, the question of whether their π-electrons are delocalized in the same sense as they are in benzene (resonance between two Kekulé structures) is less clear.

Aromaticity has many definitions. Bond-length equalization,[1] extra energetic stabilization[2] with respect to an often hypothetical reference system, and the ability to sustain an induced diatropic ring current[3-7] have all been proposed as descriptors for aromaticity. Many studies have been devoted to the aromaticity of benzene analogues using concepts of aromatic stabilization energy, exaltation of diamagnetizability Λ, and nucleus independent chemical shift (NICS[7]).[8-13] On these criteria, "inorganic benzenes" such as borazine ($B_3N_3H_6$ (**5**)), boroxine ($B_3O_3H_3$ (**9**)), and borthiin ($B_3S_3H_3$ (**10**)) are nonaromatic, whereas *s*-triphosphatriborin ($B_3P_3H_6$ (**6**)), hexaazabenzene (N_6 (**3**)), hexaphosphabenzene (P_6 (**4**)), and hexasilabenzene (Si_6H_6 (**2**)) are of modest aromatic character.[12]

* To whom correspondence should be addressed: Prof. Dr. L. W. Jenneskens. Tel: +31 302533128. Fax: +31 302534533. E-mail: l.w.jenneskens@chem.uu.nl.
  [†] Theoretical Chemistry Group, Utrecht University.
  [‡] Organic Chemistry and Catalysis, Utrecht University.
  [§] Department of Chemistry, University of Exeter.
  [||] New address from August 1, 2005: Department of Chemistry, University of Sheffield, Sheffield S3 7HF, U.K.

 (1) Cyrański, M. K.; Krygowski, T. M.; Katritzky, A. R.; von R. Schleyer, P. *J. Org. Chem.* **2002**, *67*, 1333−1338.
 (2) Cyrański, M. K.; von R. Schleyer, P.; Krygowski, T. M.; Jiao, H.; Hohlneicher, G. *Tetrahedron* **2003**, *59*, 1657−1665.
 (3) von R. Schleyer, P.; Jiao, H. *Pure Appl. Chem.* **1996**, *68*, 209−218.
 (4) Pauling, L. *J. Chem. Phys.* **1936**, *4*, 673−677.
 (5) London, F. *J. Phys. Radium* **1937**, *8*, 397−409.
 (6) Pople, J. A. *J. Chem. Phys.* **1956**, *24*, 1111.
 (7) von R. Schleyer, P.; Maerker, C.; Dransfeld, A.; Jiao, H.; van Eikema Hommes, N. J. R. *J. Am. Chem. Soc.* **1996**, *118*, 6317−6318.
 (8) Fink, W. H.; Richards, J. C. *J. Am. Chem. Soc.* **1991**, *113*, 3393−3398.
 (9) Jemmis, E. D.; Kiran, B. *Inorg. Chem.* **1998**, *37*, 2110−2116.
 (10) Cooper, D. L.; Wright, S. C.; Gerratt, J.; Hyams, P. A.; Raimondi, M. *J. Chem. Soc., Perkin Trans. 2* **1989**, *6*, 719−724.
 (11) Fowler, P. W.; Steiner, E. *J. Phys. Chem. A* **1997**, *101*, 1409−1413.
 (12) von R. Schleyer, P.; Jiao, H.; van Eikema Hommes, N. J. R.; Malkin, V. G.; Malkina, O. L. *J. Am. Chem. Soc.* **1997**, *119*, 12669−12670.
 (13) Soncini, A.; Domene, C.; Engelberts, J. J.; Fowler, P. W.; Rassat, A.; van Lenthe, J. H.; Havenith, R. W. A.; Jenneskens, L. W. *Chem. −Eur. J.* **2005**, *11*, 1257−1266.

Table 1. Energetic and Structural Data for the Set of Candidate Inorganic Benzenes

compd	R (Å)[a]	$E_{tot,B3LYP}$ (E_h)[b]	$E_{tot,RHF}$ (E_h)[b,c]	n_{imag} [d]	$\tilde{\nu}$ (cm^{-1})[e]
C_6H_6 (D_{6h}) (**1**)	1.394	−232.308558	−230.712903	0	
Si_6H_6 (D_{6h}) (**2**)	2.216	−1740.627621	−1736.868797	1 (b_{2g})	140i
N_6 (D_{6h}) (**3**)	1.319	−328.360861	−326.437481	2 (e_{2u}, b_{2u})	272i,173i
P_6 (D_{6h}) (**4**)	2.133	−2048.236337	−2044.263216	1 (e_{2u})	62i
P_6 (D_2) (**4**)	2.131	−2048.242943	−2044.268177	0	
	2.125				
$B_3N_3H_6$ (D_{3h}) (**5**)	1.431	−242.748573	−241.165102	0	
$B_3P_3H_6$ (D_{3h}) (**6**)	1.838	−1102.337952	−1099.713109	1 (a_2'')	96i
$B_3P_3H_6$ (C_{3v}) (**6**)	1.855	−1102.338684	−1099.724589	0	
$Al_3N_3H_6$ (D_{3h}) (**7**)	1.803	−895.509723	−892.779481	0	
$Al_3P_3H_6$ (D_{3h}) (**8**)	2.266	−1755.187284	−1751.462147	2 (e'', a_2'')	166i,151i
$Al_3P_3H_6$ (C_s) (**8**)	2.296	−1755.201278	−1751.471417	0	
	2.316				
	2.314				
$B_3O_3H_3$ (D_{3h}) (**9**)	1.377	−302.403016	−300.701018	0	
$B_3S_3H_3$ (D_{3h}) (**10**)	1.809	−1271.176315	−1268.490842	0	

[a] Ring bond length. [b] B3LYP optimized within symmetry constraints (see text). Total energies at B3LYP/**basis1** ($E_{tot,B3LYP}$) and RHF/6-31G** ($E_{tot,RHF}$) levels. [c] RHF/6-31G** energy calculated at the B3LYP/**basis1** optimized geometry. The σ-orbitals from this calculation are retained in the VB procedure. [d] Number of imaginary frequencies. The symmetries of the imaginary modes are indicated between parentheses. [e] Corresponding wavenumbers ($\tilde{\nu}$) for compounds **1**−**10**. See Supporting Information.

An important question is whether the electronic structure of an inorganic benzene expressed in terms of Lewis structures resembles that of benzene itself. The valence bond (VB) theory,[14] where a molecular wave function is constructed from atomic states, offers an interpretation precisely in terms of resonating Lewis structures.[15] Weights can be attributed to these structures, using a formula proposed by Chirgwin and Coulson to assess their importance in the total wave function.[16] Furthermore, the VB theory provides a resonance energy (E_{res}) of a molecule, as defined by Pauling;[17] this is the difference between the total energy (E_{tot}) and that of the most stable structure. For benzene itself, a large value of $E_{res} = 85$−190 kJ/mol with respect to one structure is found.[18−20] The structure with the lowest energy is of the Kekulé type and has the largest weight in the wave function. Thus, for benzene (**1**), aromaticity is characterized not only by a high resonance energy but also by large weights of the Kekulé structures in the wave function.

In contrast, for the heteronuclear analogues borazine (**5**) and boroxine (**9**), spin-coupled valence bond calculations indicate that only one Lewis structure, corresponding to a description of three lone pairs localized on the electronegative centers, is important in the wave function, and E_{res} is negligible.[10] Significantly, the negligible resonance energy coincides with the absence of a diatropic π ring current, and so energetic and magnetic criteria of aromaticity are in agreement here.[11]

The aim of the present paper is to explore the parallels between the energetic and magnetic criteria of aromaticity for a series of inorganic benzenes, using VB methods for

evaluation of resonance energy (E_{res}) and distributed origin computation of induced current density to establish the presence or absence of ring currents. VB calculations are performed using both the strictly atomic model and the spin-coupled method. The magnetic response treatment is carried out at the coupled Hartree−Fock level[21,22] using the "ipso-centric"[23,24] CTOCD-DZ[25] approach, which is derived from the continuous set of gauge transformations (CSGT) method of Keith and Bader[26] and which provides maps of induced current density that give detailed information about the nature and distribution of currents and rationalize other magnetic indices of aromaticity.

A set of candidate inorganic benzenes was defined (with benzene itself included for comparison) as X_6H_6 (X = C(**1**), Si (**2**)), X_6 (X = N (**3**), P (**4**)), $X_3Y_3H_6$ (X,Y = B,N (**5**), B,P (**6**), Al,N (**7**), Al,P (**8**)), and $B_3Y_3H_3$ (Y = O (**9**), S (**10**)). Computed data on electric[27] and magnetic[12] properties of some of the molecules in the set are available in the literature, including a full set of NICS(0)[7] values for all of the molecules studied here.

2. Computational Details

2.1. Geometry Optimization. Geometries of the molecules were optimized with GAMESS-UK[28] at the density functional theory (DFT) level, using the B3LYP functional (Table 1).[29−31] For

(14) Heitler, W.; London, F. *Z. Phys.* **1927**, *44*, 455−472.
(15) Lewis, G. N. *J. Am. Chem. Soc.* **1916**, *38*, 762−785.
(16) Chirgwin, B. H.; Coulson, C. A. *Proc. R. Soc. London, Ser. A* **1950**, *201*, 196−209.
(17) Pauling, L.; Wheland, G. W. *J. Chem. Phys* **1933**, *1*, 362−374.
(18) van Lenthe, J. H.; Havenith, R. W. A. Dijkstra, F.; Jenneskens, L. W. *Chem. Phys. Lett.* **2002**, *361*, 203−208.
(19) Cooper, D. L.; Gerratt, J.; Raimondi, M. *Nature* **1986**, *323*, 699−701.
(20) Dijkstra, F.; van Lenthe, J. H.; Havenith, R. W. A.; Jenneskens, L. W. *Int. J. Quantum Chem.* **2003**, *91*, 566−574.

(21) Keith, T. A.; Bader, R. F. W. *J. Phys. Chem. A* **1993**, *99*, 3669−3682.
(22) Lazzeretti, P.; Malagoli, M.; Zanasi, R. *Chem. Phys. Lett.* **1994**, *200*, 299−304.
(23) Steiner, E.; Fowler, P. W. *J. Phys. Chem. A* **2001**, *105*, 9553−9562.
(24) Steiner, E.; Fowler, P. W. *Chem. Commun.* **2001**, 2220−2221.
(25) Zanasi, R. *J. Chem. Phys.* **1996**, *105*, 1460−1469.
(26) Keith, T. A.; Bader, R. F. W. *Chem. Phys. Lett.* **1993**, *210*, 223−231.
(27) Lazzeretti, P.; Tossell, J. A. *J. Mol. Struct. (THEOCHEM)* **1991**, *236*, 403−410.
(28) GAMESS-UK is a package of ab initio programs written by M. F. Guest, J. H. van Lenthe, J. Kendrick, K. Schoffel, and P. Sherwood, with contributions from R. D. Amos, R. J. Buenker, H. J. J. van Dam, M. Dupuis, N. C. Handy, I. H. Hillier, P. J. Knowles, V. Bonacic-Koutecky, W. von Niessen, R. J. Harrison, A. P. Rendell, V. R. Saunders, A. J. Stone, D. J. Tozer, and A. H. de Vries. The package is derived from the original GAMESS code. Dupuis, M.; Spangler, D.; Wendoloski, J. *NRCC Software Catalog*, Vol. 1; program no. QG01 (GAMESS), 1980.

hydrogen, boron, carbon, and nitrogen the 6-311^{++}G** basis[32−34] was used, and for the aluminum, phosphorus, sulfur, and silicon the 6-311G**[35,33] basis was used. We refer to this combination as **basis1**. Heteronuclear rings were constrained to D_{3h} symmetry and homonuclear rings to D_{6h} symmetry. Hessian calculations show the planar symmetric geometries of **1**, **5**, **7**, **9**, and **10** to correspond to genuine minima on the potential energy surface at this level of theory. For **2**, **3**, **4**, **6**, and **8**, one (or more) imaginary frequencies were found, indicating that the constrained structures are transition states (or higher order saddle points). These results are in agreement with earlier data.[36−40] The relaxation of Si_6H_6 (**2**) from D_{6h} to D_{3d} symmetry is accompanied with a change in the NICS(0) value from −13.1 into −11.0,[41] indicating that the aromatic character is retained. N_6 (**3**) is not stable and dissociates into three separate N_2 molecules,[38] and **8** in the D_{3h} geometry shows no aromatic character, a feature which will not change for the optimal C_s symmetry conformation. Therefore, only the D_{6h} conformations of **2** and **3** and the D_{3h} conformation of **8** are studied here. The e_{2u} symmetry of the imaginary frequency for D_{6h}-P_6 (**4**) suggests an out-of-plane distortion to D_2, and both conformations are studied. For **6**, both the D_{3h} and the chair (C_{3v}) conformation, which corresponds to the minimum on the potential energy surface, are investigated.

2.2. Valence Bond Calculations. VB/6-31G**[32,35,42−44]//B3LYP/ **basis1** calculations were performed with TURTLE[45] as implemented in the GAMESS-UK package.[28] In all of the calculations, frozen σ orbitals were taken from a preceding RHF/6-31G** calculation, and the π system was described by six atomic p-orbitals. Two types of calculations were carried out, viz., strictly atomic and spin coupled.

In the strictly atomic model, the orbitals were optimized using the valence bond self-consistent field (VBSCF)[46,47] but were forced to remain on their initial centers throughout the optimization. The advantage of this model is its clear interpretability in terms of well-defined Lewis structures. Since the X and Y atoms can contribute 0, 1, or 2 electrons to the π system in a general $X_3Y_3H_n$ cycle, the wave function was accordingly constructed from Lewis structures representing, respectively, the two Kekulé terms (**I** and **II**), three lone pairs on X (**III**), and three lone pairs on Y (**IV**) (Figure 1).
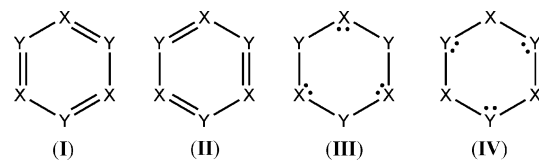
(29) Lee, C.; Yang, W.; Parr, R. G. *Phys. Rev. B* **1988**, *37*, 785−789.
(30) Becke, A. D. *J. Chem. Phys.* **1993**, *98*, 1372−1377.
(31) Becke, A. D. *J. Chem. Phys.* **1993**, *98*, 5648−5652.
(32) Binkley, J. S.; Pople, J. A.; Hehre, W. J. *J. Am. Chem. Soc.* **1980**, *102*, 939−947.
(33) Krishnan, R.; Binkley, J. S.; Seeger, R.; Pople, J. A. *J. Chem. Phys.* **1980**, *72*, 650−654.
(34) Clark, T.; Chandrasekhar, J.; von R. Schleyer, P. *J. Comput. Chem.* **1983**, *4*, 294−301.
(35) Gordon, M. S.; Binkley, J. S.; Pople, J. A.; Pietro, W. J.; Hehre, W. J. *J. Am. Chem. Soc.* **1982**, *104*, 2797−2803.
(36) Matsunaga, N.; Gordon, M. S. *J. Am. Chem. Soc.* **1994**, *116*, 11407−11419.
(37) Doerksen, R. J.; Thakkar, A. J. *J. Phys. Chem. A* **1998**, *102*, 4679−4686.
(38) Nagase, S.; Ito, K. *Chem. Phys. Lett.* **1986**, *126*, 43−47.
(39) Tobita, M.; Bartlett, R. J. *J. Phys. Chem. A* **2001**, *105*, 4107−4113.
(40) Nagase, S.; Teramae, H.; Kudo, T. *J. Chem. Phys.* **1987**, *86*, 4513−4517.
(41) Baldridge, K. K. *Organometallics* **2000**, *19*, 1477−1487.
(42) Hehre, W. J.; Ditchfield, R.; Pople, J. A. *J. Chem. Phys.* **1972**, *56*, 2257−2261.
(43) Dill, J. D.; Pople, J. A. *J. Chem. Phys.* **1975**, *62*, 2921−2923.
(44) Francl, M. M.; Pietro, W. J.; Hehre, W. J.; Binkley, J. S.; Gordon, M. S.; DeFrees, D. J.; Pople, J. A. *J. Chem. Phys.* **1982**, *77*, 3654−3665.
(45) Verbeek, J.; Langenberg, J. H.; Byrman, C. P.; Dijkstra, F.; Engelberts, J. J.; van Lenthe, J. H. *TURTLE, an ab initio VB/VBSCF program*; 1988−2004.
(46) van Lenthe, J. H.; Balint-Kurti, G. G. *Chem. Phys. Lett.* **1980**, *76*, 138−142.
(47) van Lenthe, J. H.; Balint-Kurti, G. G. *J. Chem. Phys.* **1983**, *78*, 5699−5713.

Figure 1. The four structures used in strictly atomic VBSCF.

To partition the resonance energy (E_{res}) into resonance interactions between pairs of structures, the structures are orthogonalized using the criterion of maximum overlap (Löwdin orthogonalization[48]). The total energy (E_{tot}) can be divided into contributions from the orthogonalized structures and their π-electron interactions (resonances).[49] The contribution of Kekulé-type resonance to the resonance energy (E_{res}) can then be expressed as a percentage of the total orthogonalized resonance energy.

The spin-coupled valence bond wave function comprises one configuration with all of the possible spin couplings (two Kekulé and three Dewar structures), and the orbitals are optimized without any restrictions.[50,51]

2.3. Calculation of the Induced Current Density. Magnetic properties for all 10 compounds were calculated with SYSMO[52] at the coupled Hartree−Fock level within the CTOCD-*DZ* formalism[21−26] and using the 6-31G** basis set[32,35,42−44] in the planar and planar-constrained geometries. Maps of σ, π, and total ($\sigma + \pi$) contributions to the current density were obtained. The current density, induced by a unit magnetic field directed along the principal axis, is plotted in a plane $1a_0$ above and parallel to the molecular plane. Diatropic circulation is shown counterclockwise. As a quantitative indicator, the maximum magnitude of the current density over each bond midpoint was determined for D_{6h} **1**−**4** in a square of dimension 2×2 a_0 centered on the point midway between two neighboring atoms of the ring. For the maps of **4** and **6** in their nonplanar, optimal structures, use was made of Pipek−Mezey[53] localized orbitals in order to distinguish between the P−P single bonds and the π-type orbitals. The sum of the contributions of the three π-type orbitals to the current density is plotted in various planes (see text).[54] Magnetic shielding values at the ring center (−NICS(0)[7]) were obtained by integration of the full three-dimensional induced current density for the three directions of the external field, using the CTOCD-*PZ2* formalism.[55,56]

3. Results

3.1. Valence Bond. The results from the strictly atomic VBSCF calculations are reported in Table 2. For the X_6 ring compounds **1**−**4**, large weights for the Kekulé structures (W (**I**) and W (**II**)) and resonance energies E_{res} ranging from 53.7 to 161.4 kJ/mol are found.

With the exception of **6**, the heteronuclear ring compounds have a low weight for the Kekulé structures. The lone-pair

(48) Löwdin, P. O. *Rev. Mod. Phys.* **1967**, *39*, 259−287.
(49) Havenith, R. W. A.; van Lenthe, J. H.; Dijkstra, F.; Jenneskens, L. W. *J. Phys. Chem. A* **2001**, *105*, 3838−3845.
(50) Gerratt, J.; Raimondi, M. *Proc. R. Soc. London, Ser. A* **1980**, *371*, 525−552.
(51) Cooper, D. L.; Gerratt, J.; Raimondi, M. *Adv. Chem. Phys.* **1987**, *69*, 319−397.
(52) Lazzeretti, P.; Zanasi, R. *SYSMO package (University of Modena); 1980.* Additional routines, Steiner, E., Fowler, P. W., and Havenith, R. W. A.
(53) Pipek, J.; Mezey, P. G. *J. Chem. Phys.* **1989**, *90*, 4916−4926.
(54) Steiner, E.; Fowler, P. W.; Havenith, R. W. A. *J. Phys. Chem. A* **2002**, *106*, 7048−7056.
(55) Zanasi, R.; Lazzeretti, P.; Malagoli, M.; Piccinini, F. *J. Chem. Phys.* **1995**, *102*, 7150−7157.
(56) Soncini, A.; Fowler, P. W. *Chem. Phys. Lett.* **2004**, *396*, 174−181.

Table 2. The Total Energy (E_{tot}) of the Four Structure Strictly Atomic VBSCF Calculations, the Corresponding Resonance Energy (E_{res}), and the Contribution of the Resonance between the Orthogonalized Kekulé Structures to the Orthogonalized Resonance Energy (%)

compound	E_{tot} (E_h)	E_{res} (kJ/mol)	%	W (**I**)[a]	W (**II**)[a]	W (**III**)[a]	W (**IV**)[a]
C_6H_6 (D_{6h}) (**1**)	−230.632723	161.4	42	0.47	0.47	0.03	0.03
Si_6H_6 (D_{6h}) (**2**)	−1736.843163	71.3	46	0.48	0.48	0.02	0.02
N_6 (D_{6h}) (**3**)	−326.352653	138.8	59	0.49	0.49	0.01	0.01
P_6 (D_{6h}) (**4**)	−2044.248814	53.7	69	0.49	0.49	0.01	0.01
$B_3N_3H_6$ (D_{3h}) (**5**)	−241.032610	61.6	7	0.05	0.05	0.90	0.00
$B_3P_3H_6$ (D_{3h}) (**6**)	−1099.608270	132.6	17	0.21	0.21	0.58	0.00
$Al_3N_3H_6$ (D_{3h}) (**7**)	−892.689102	12.5	3	0.01	0.01	0.98	0.00
$Al_3P_3H_6$ (D_{3h}) (**8**)	−1751.396664	18.2	6	0.02	0.02	0.96	0.00
$B_3O_3H_3$ (D_{3h}) (**9**)	−300.569045	27.6	4	0.02	0.02	0.96	0.00
$B_3S_3H_3$ (D_{3h}) (**10**)	−1268.385041	34.3	7	0.04	0.04	0.92	0.00

[a] The last four columns contain the weights of the Kekulé structures (**I** and **II**) and the lone-pair structures (**III** and **IV**) (Figure 1).

Table 3. Total Energy (E_{tot}) and Resonance Energy (E_{res}) from the Spin-Coupled Orbital VBSCF Calculations for **1**−**10**

compound	E_{tot} (E_h)	E_{res} (kJ/mol)
C_6H_6 (D_{6h}) (**1**)	−230.778804	81.4
Si_6H_6 (D_{6h}) (**2**)	−1736.915636	43.3
N_6 (D_{6h}) (**3**)	−326.543850	97.8
P_6 (D_{6h}) (**4**)	−2044.335507	47.1
$B_3N_3H_6$ (D_{3h}) (**5**)	−241.203143	0.7
$B_3P_3H_6$ (D_{3h}) (**6**)	−1099.736541	52.5
$Al_3N_3H_6$ (D_{3h}) (**7**)	−892.818391	0.0
$Al_3P_3H_6$ (D_{3h}) (**8**)	−1751.476886	0.2
$B_3O_3H_3$ (D_{3h}) (**9**)	−300.744566	0.1
$B_3S_3H_3$ (D_{3h}) (**10**)	−1268.507409	1.3

structure with two electrons on each atom X (**III**), Figure 1, is dominant in the wave function (highest weight varying from 0.90 to 0.98). E_{res} varies from 12.5 to 61.6 kJ/mol, except in **6**, for which a substantially higher resonance energy (E_{res}) of 132.6 kJ/mol is found. The contributions to the resonance energy of the resonance between the orthogonalized Kekulé structures are between 3 and 7% but 17% for **6**.

In Table 3, the results from the spin-coupled VB calculations are presented. Whereas E_{res} is still appreciable for the homonuclear rings, it is close to zero for the heteronuclear rings **5** and **7**−**10** but significant for **6**. All of the E_{res} values are lower than those obtained for the strictly atomic orbital model.

Figure 2 shows the two singly occupied p-orbitals of benzene (**1**), borazine (**5**), and s-triphosphatriborin (**6**), respectively. After the optimization of the spin-coupled wave function, **1** and **6** show one p-orbital per atom with tails on both neighboring atoms, that is, only a minor change from the starting position of a single p-orbital per atom. For **5**, the orbital that originated from a boron atom migrates completely to the nitrogen atom, leaving only small tails on the neighboring boron atoms (cf. ref 10).

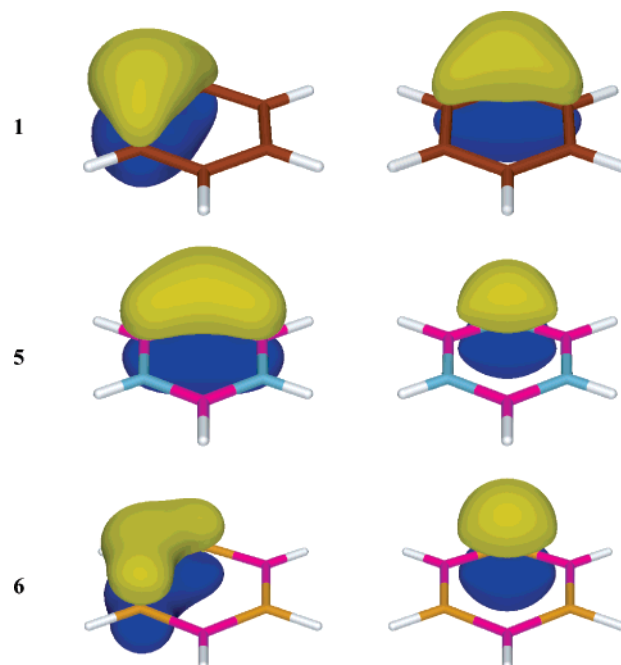**3.2. Ring Currents.** From the plots of induced π-current density, computed in the ipsocentric approach, it can be

Figure 2. A p-electron pair of C_6H_6 (**1**), $B_3N_3H_6$ (**5**), and $B_3P_3H_6$ (**6**) from top to bottom. Note that each spin-coupled calculations started with one p-orbital on each (hetero) atom.

deduced that the homonuclear rings support appreciable diatropic ring currents (Figure 3). In contrast, the maps for the heteronuclear ring compounds show in all but one case, viz., **6**, islands of localized currents centered around the electronegative atoms X. In the special case, **6**, there is a discernible diatropic π ring current. The maps for **5** and **9** are similar to those previously reported.[11,54]

Sample σ and total ($\sigma + \pi$) current-density maps for **1**, **3**, **6**, and **7** are shown in Figure 4. Benzene (**1**) and N_6 (**3**) show the profile familiar from many monocyclic and polycyclic compounds: superposition of localized diatropic σ-bond currents leads to an outer diatropic circulation and an inner paratropic central circulation within the ring. The localized compound **7** shows a different σ profile, with three localized circulations around the electronegative centers and no significant global perimeter circulation. In this context, **6** appears again as a transitional system, with a pattern that shows a tendency for the localization of currents over the electronegative phosphorus atoms but with vestigial perimetric diatropic circulation. Total ($\sigma + \pi$) maps at a height of $1a_0$ are dominated by the π ring currents in the homonuclear rings **1** and **3** and by the reinforcing lone-pair localized currents in **7**. Again, **6** has a transitional character, with counterrotating perimetric and central currents but without pronounced π or σ-global ring current. Figure 5 shows what happens to the π ring current of **6** on relaxation to its optimal structure. The contribution of the orbitals derived from the π orbitals of the planar structure change from a global circulation to a set of localized islands, corresponding to the axial lone pairs of the phosphorus atoms.

Shieldings at the ring center (cf. −NICS(0) values) and the maximum magnitudes of π-current density (j_{max}) for the homonuclear rings are reported in Table 4. Broad agreement
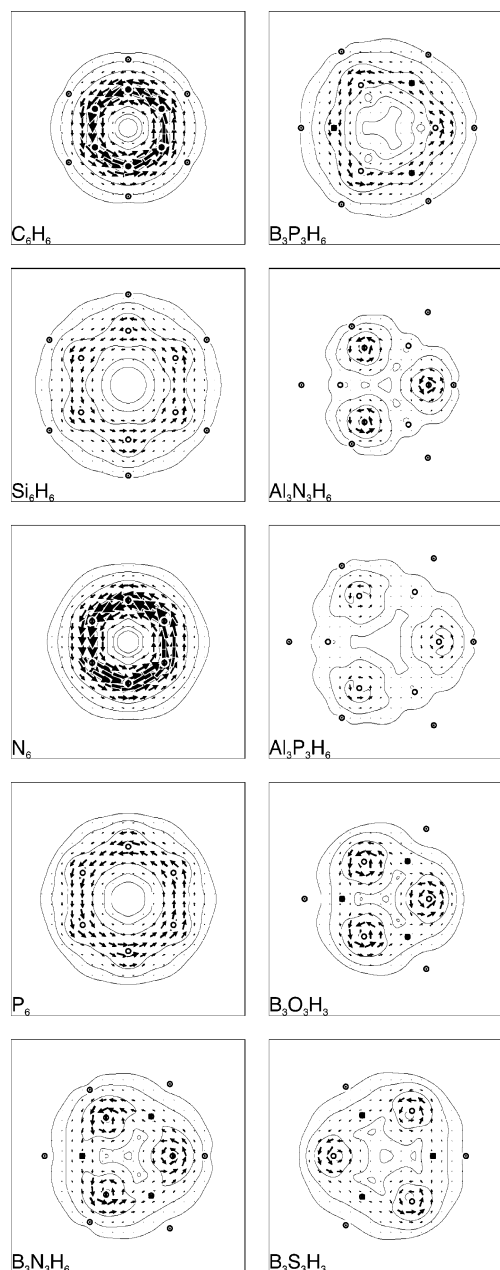
Figure 3. Maps of π-current density induced by a perpendicular magnetic field in planar geometries of compounds **1**−**10**. Current is plotted in a plane 1 a_0 above the nuclei, with counterclockwise arrows indicating diatropic circulation.

Figure 4. Maps of the σ (left) and the total ($\sigma + \pi$) (right) current density induced by a perpendicular magnetic field in planar geometries of compounds **1**, **3**, **6**, and **7** (from top to bottom). Current is plotted in a plane 1 a_0 above the nuclei, with counterclockwise arrows indicating diatropic circulation.

in size and sign is seen between CTOCD-*PZ2* mean shieldings and those previously reported,[12] despite differences in the basis set, treatment of gauge, and level of electronic structure theory. An exception is the planar transition state structure of P_6 (**4**), which shows, among others, a pronounced dependence on the basis set.[57] When discussing π ring currents, perhaps more significant than the value of the average shielding is the out-of-plane component of the shielding tensor, σ_{zz}, as this component reflects the effect of a perpendicular magnetic field.[59−61] The σ_{zz} is calculated to

be positive for all of the homonuclear rings in the set but negative for the heteronuclear compounds. Interestingly, $B_3P_3H_6$ (**6**) shows a near-zero computed value of σ_{zz} (vide infra).

4. Discussion

4.1. Homonuclear X_6H_n Series. The four homonuclear compounds show "aromatic" behavior on both electronic

(57) A CTOCD-*PZ2* calculation with the larger Sadlej[58] basis set resulted in $-\sigma_{ip} = -4.6$, $-\sigma_{zz} = -20.5$, and $-\sigma_{av} = -9.9$. Note that only for P_6 (**4**), besides the basis set dependency, a method dependency is found as well.
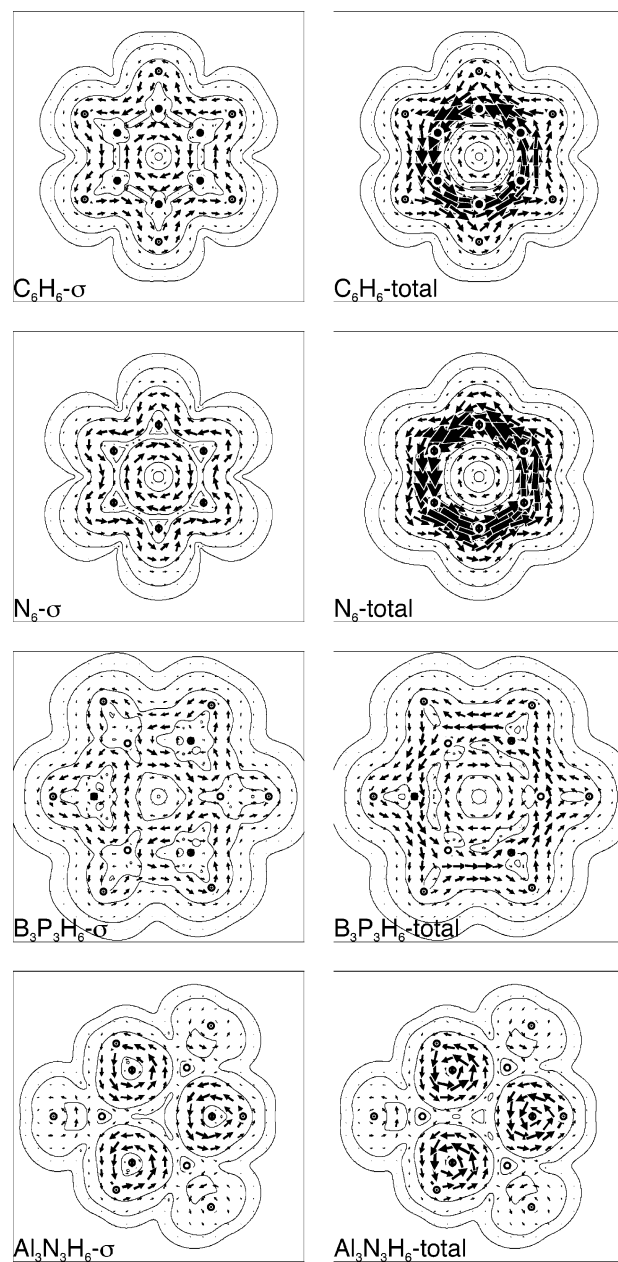(58) Sadlej, A. J. *Theor. Chim. Acta* **1991**, *79*, 123−140.

(59) Steiner, E.; Fowler, P. W.; Jenneskens, L. W. *Angew. Chem., Int. Ed.* **2001**, *40*, 362−366.
(60) Corminboeuf, C.; Heine, T.; Seifert, G.; von R. Schleyer, P.; Weber, J. *Phys. Chem. Chem. Phys.* **2004**, *6*, 273−276.
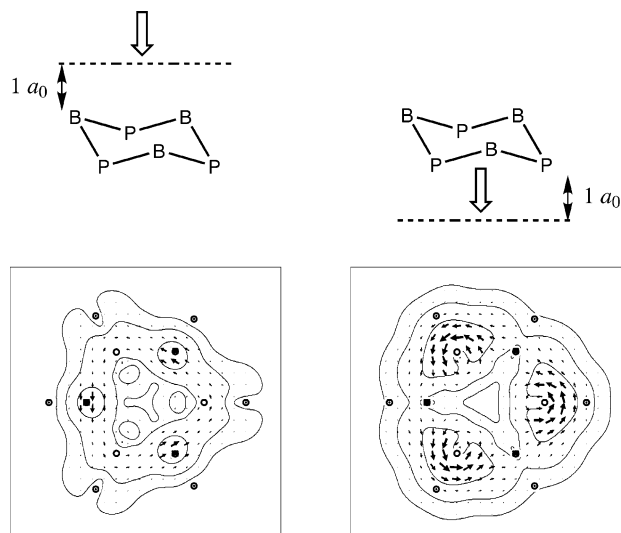(61) Viglione, R. G.; Zanasi, R.; Lazzeretti, P. *Org. Lett.* **2004**, *6*, 2265−2267.

Figure 5. Maps of the induced π-current density induced by a magnetic field acting along the principal axis for $B_3P_3H_6$ (**6**) in optimal C_{3v} symmetry plotted in a plane $1a_0$ above the plane of boron nuclei (left) and $1a_0$ below the plane of phosphorus nuclei (right) the molecule. The pictures above the maps indicate the plotting plane (dashed lines), and the open arrow indicates the direction of view.

Table 4. CTOCD-*PZ2* Components of the Magnetic Shieldings (σ) Calculated at the Ring Center, Isotropic Average, Literature NICS(0) Values, and j_{max} for the Studied Compounds (**1**–**10**)

compound	$-\sigma_{ip}$ [a]	$-\sigma_{zz}$	$-\sigma_{av}$ [b]	NICS(0) [c]	j_{max} [d]
C_6H_6 (D_{6h}) (**1**)	−11.0	−16.4	−12.8	−8.9	0.078
Si_6H_6 (D_{6h}) (**2**)	−10.9	−16.7	−12.8	−13.1	0.022
N_6 (D_{6h}) (**3**)	1.8	−1.1	0.9	0.2	0.089
P_6 (D_{6h}) (**4**)	6.9	−14.2	−0.1	−15.2	0.031
P_6 (D_2) (**4**)	7.5	−22.7	−2.6		
$B_3N_3H_6$ (D_{3h}) (**5**)	−9.7	13.4	−2.0	−2.1	
$B_3P_3H_6$ (D_{3h}) (**6**)	−12.9	1.1	−8.2	−8.7	
$B_3P_3H_6$ (C_{3v}) (**6**)	−13.9	5.5	−7.4		
$Al_3N_3H_6$ (D_{3h}) (**7**)	−8.9	11.1	−2.2	−2.4	
$Al_3P_3H_6$ (D_{3h}) (**8**)	−11.7	4.6	−6.3	−5.8	
$B_3O_3H_3$ (D_{3h}) (**9**)	−8.0	20.0	1.4	−0.8	
$B_3S_3H_3$ (D_{3h}) (**10**)	−13.2	11.4	−5.0	−2.5	

[a] In-plane average $\sigma_{ip} = (1/2) (\sigma_{xx} + \sigma_{yy})$. [b] Isotropic average for compounds **1**–**10**. [c] Taken from ref 12. [d] Maximum modulus of the current density.

structure and magnetic indicators. A survey of the strictly atomic model results shows that **1**–**4** have large Kekulé resonance contributions above 40% and high Kekulé structure weights ($W(\mathbf{I}) = W(\mathbf{II})$), though explicit addition of Lewis structures **III** and **IV** increases the resonance energy, as it must by the variation principle. In the case of benzene, the inclusion of **III** and **IV**, which gives an improvement of the wave function that is outside the classical Kekulé resonance picture, amounts to an increase of about 52 kJ/mol. All four molecules also display diatropic π ring currents, as expected for aromatic compounds, and there is qualitative correlation between the strength of current (j_{max}) and the size of the resonance energy (Table 2). C_6H_6 (**1**) and planar N_6 (**3**) show strong ring currents and resonance energies (E_{res}) of 161.4 and 138.8 kJ/mol; planar **2** and **4** show ring currents of less than half the benzene strength and resonance energies (E_{res}) of 71.3 and 53.7 kJ/mol. The spin-coupled model shows lower resonance energies (E_{res}) than the strictly atomic method. In spin-coupled VB, the orbitals have the freedom to spread out, which means the implicit inclusion of ionic
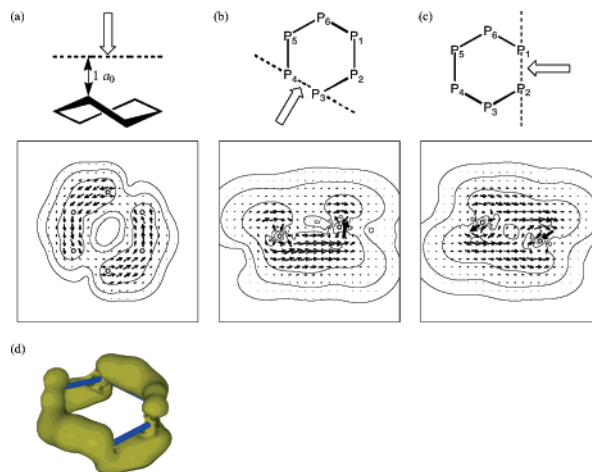
Figure 6. Maps of the induced π-current density induced by a magnetic field acting perpendicular to the median plane for P_6 (**4**) in optimal D_2 symmetry plotted in a plane (a) $1a_0$ above the top 2 phosphorus nuclei, (b) containing the P_3–P_4 bond and the magnetic field, and (c) containing the P_1–P_2 bond and the magnetic field and (d) contour plot of the modulus of π-current-density (contour value: 0.024). Diatropic current is denoted by arrows pointing counterclockwise (a) and from left to right (b) and (c). The pictures above the maps indicate the plotting plane (dashed lines), and the open arrow indicates the direction of view.

bond character. The only way to include ionic character in the strictly atomic model is to mix the lone-pair structures **III** and **IV** into the Kekulé picture of the homonuclear compounds and to mix the Kekulé-type structures **I** and **II** into the lone-pair description of the heteronuclear compounds. E_{res} is defined as the difference between the energy of the most stable structure and the total energy (E_{tot}). The most stable spin-coupled structure has a lower energy than the most stable structure in the strictly atomic model, leading to a higher E_{res} for the strictly atomic model.

Interestingly, the magnetic aromaticity of **3** is not captured by calculating the NICS(0) index. As has been discussed elsewhere,[62] the isotropic central shielding that defines NICS is influenced by many factors in addition to the π ring currents; even restriction to the out-of-plane component of shielding does not help here, as localized σ- and delocalized π-circulations give near canceling contributions to σ_{zz}. Inspection of the current-density map is more informative than either of these global integral properties.

The ring-current calculations on **4** require a more detailed explanation: although $-\sigma_{av}$ is only −0.1 for planar **4**, the π map in Figure 3 shows a strong ring current, and consistent with this observation, the $-\sigma_{zz}$ component is −14.2, indicating aromatic character. For the method and basis set used here, the paratropic in-plane component of NICS exactly counteracts the diatropic ring-current component, whereas an enlargement of the basis set leads to a similar $-\sigma_{zz}$ but different in-plane average ($-\sigma_{ip}$) value (see also ref 57).

The deformation to the optimal D_2 symmetric geometry of **4** does not quench the π ring current, as shown in Figure 6. The side view plots through the two symmetry unique P_1–P_2 and P_3–P_4 bonds show that the main current along the P_3–P_4 bond is concentrated on one side of the bond,

(62) Steiner, E.; Fowler, P. W. *Phys. Chem. Chem. Phys.* **2004**, *6*, 261–272.

while along the P_1-P_2 bond it is more evenly distributed. A contour plot of the modulus of π-current density (contour value of 0.024) gives an indication of the current path in three dimensions (as do the arrows sometimes added to the plots of current-density anisotropy in the ACID method[63]). This picture combined with the side view plots show the continuous π ring current and rationalize the gaps seen in the map plotted $1.6a_0$ above and parallel to the median plane.

4.2. Heteronuclear $X_3Y_3H_n$ Series. Our calculations give little support to any putative assignment of these compounds as being "aromatic". All but $B_3P_3H_6$ (**6**) fit into a simple pattern: they have low resonance energies (E_{res}) and large weights for a localized lone-pair structure with low-fractional contributions of Kekulé resonances to E_{res}. Maps of induced current density show concomitant localization of the magnetic response.

Borazine (**5**) appears to be an exception to this pattern. In the strictly atomic VB calculations, it shows a significant E_{res} value of 61.6 kJ/mol. Upon relaxation of the constraint on the nature of the p-orbitals, however, this E_{res} value is seen to have been an artifact. The improved E_{res} value, available from the spin-coupled VB calculation, is negligible (0.7 kJ/mol). The maps (Figure 3) do not show any evidence of benzenoid behavior.

In contrast, **6** possesses a large resonance energy both in the strictly atomic and in the spin-coupled VBSCF calculations, but its $-\sigma_{zz}$ value is 1.1. As shown in the maps in Figures 3 and 4, in the case of **6**, the weak diatropic π current is canceled by paratropic contributions (see also **3**), because of localized σ currents. The average in-plane component of NICS(0), notwithstanding, is negative ($-\sigma_{ip} = -12.9$), leading to an aromatic overall $-\sigma_{av}$ value (NICS(0)) of -8.2. Hence, for **6** total NICS(0) does not reflect the presence of an underlying ring current. An interesting critique of the NICS approach in general is given in ref 64.

The exceptional character of **6** is also reflected by the contour plots of its spin-coupled orbitals in comparison with those of benzene (**1**) and borazine (**5**) (Figure 2). While for benzene (**1**), one singly occupied orbital on each carbon atom is found, which can be interpreted as a covalent bond, for borazine (**5**) two singly occupied orbitals centered on nitrogen are discernible, which correspond to the description of a nitrogen lone pair. $B_3P_3H_6$ (**6**) is formally more similar to borazine (**5**), but its orbitals are intermediate between those of benzene (**1**) and borazine (**5**): one orbital is strictly centered on phosphorus (similar to **5**), while the other orbital is centered on boron (more benzenoid) with tails on phosphorus, representing the larger Kekulé-type structure contributions because of the small difference in electronegativity between boron and phosphorus.[65] Thus, this pictorial result, together with the E_{res} of 52.5 kJ/mol and the large

Kekulé resonance contribution to the orthogonalized resonance energy, suggests that planar **6** is benzene-like.

The current-density maps give an indication of aromatic behavior in *planar* **6** in that the π-current pattern is delocalized, though not uniform in strength. When the geometry is allowed to relax to the local C_{3v} minimum, the current changes from a global circulation to a set of localized islands, corresponding to the *axial* lone pairs of the phosphorus atoms (Figure 6). Thus, **6** is nonaromatic, according to the magnetic criterion.

5. Conclusions

Three complementary theoretical techniques were used to explore the putative aromaticity of a set of inorganic benzenes. Each technique gives a visualization of aromaticity: strictly atomic VB calculations through the balance of Kekulé and lone-pair structures, spin-coupled calculations through resonance energy, and the CTOCD-*DZ* current-density maps through the distinction between global ring-current and local circulations.

The strictly atomic model gives a clear division of the molecules into a benzene-like group and a group with lone pairs on the most electronegative atoms. This division corresponds to that derived from the maps of magnetic response. The spin-coupled method, which gives an improved description of the electronic structure through unrestricted orbital optimization, leads to the same partitioning of the set. If the label "inorganic benzene" is to be applied to any of the compounds studied, it is apparently appropriate only for the homonuclear ring compounds and the constrained **3** and with reservations, for the planar geometry of **6**.

Note Added after ASAP Publication. There were errors in the footnotes of Tables 1 and 4 in the version published ASAP June 14, 2005; the corrected version was published June 23, 2005.

Supporting Information Available: Cartesian coordinates for B3LYP/**basis1** (non)-constrained compounds **1**−**10**. This material is available free of charge via the Internet at http://pubs.acs.org.

IC050017O

(63) Herges, R.; Geuenich, D. *J. Phys. Chem. A* **2001**, *105*, 3124−3220.

(64) Lazzeretti, P. *Phys. Chem. Chem. Phys.* **2004**, *6*, 217−223.
(65) Pauling, L. *J. Am. Chem. Soc.* **1932**, *54*, 3570−3582.